PMMA Additive-Induced Active Layer Self-Assembly in Polymer Solar Cells: Towards Low-Cost, Ultra-Portable, Mass-Produced Solar Energy

Abstract: Although polymer solar cells show potential as an alternative energy source due to their low cost, light weight, and flexibility, they remain unviable for mass-production because their active layer films are currently too thin. This project thus develops a method of increasing thickness while maintaining efficiency through additive-induced columnar self-assembly. After a survey of parameters for nine polymers, PMMA was chosen for testing due to its favorable solubility, surface energy, strength, and price. Ellipsometry demonstrated an increase in film thickness and atomic force microscopy (AFM) confirmed the columnar structure for improved charge conduction. This improvement in morphology resulted in a 33.7% increase in power conversion efficiency (PCE) relative to the control. A 68.0% increase in external quantum efficiency (EQE) was noted, prompting further research on the role of light trapping in PMMA-enhanced solar cells. A simulation model of light absorbance and reflectance in the cell was created in C++ with parameters based on AFM images, which predicted an increase in light absorption, confirming the role of light trapping in the improved active layer blend EQE. Thus, PMMA was demonstrated as a morphology-optimizing additive in the active layer, which is key to mass-production of polymer solar cells.

1. Introduction:

An alternative energy source to fossil fuels is critical for reducing greenhouse gas and air pollutant emissions, halting anthropogenic climate change, and promoting energy independence (Edenhofer, 2011). Although today's commercially available photovoltaics have become price competitive with fossil fuels, they are limited in the ways that they can be implemented and have high manufacturing and installation costs (Edenhofer, 2011). The developing technology of polymer solar cells offers a possible solution to these issues: they are light, flexible, and semitransparent, allowing for a range of novel applications of solar energy such as energy-harvesting windows, and they can be fabricated in ambient conditions using a roll-to-roll printing technique, thus vastly reducing manufacture cost and environmental impact of production. (Li, 2012; Hoppe, 2007; Scharber, 2013; Søndergaard, 2012). However, despite the promise that polymer solar cells show, much work remains to be done in improving scalability, which is limited by the thinness of the active layer, and their low power conversion efficiencies, which lag behind those of their inorganic counterparts (Hoppe, 2007; Lee, 2010; Peet, 2011; Li, 2012; Li, 2013; Heeger, 2013; Etxeberria, 2015; Zhang, 2017).

The thickness measurement of the active layer—the component of the cell that absorbs photons and generates electricity—is a crucial parameter that is holding back the mass-production of polymer solar cells (Lee, 2010; Peet, 2011; Li, 2013). The active layer is composed of a polymer blend of an electron donor and an electron acceptor which, upon absorbing a photon, creates a bound electron-hole pair that generates electricity when conducted to the electrodes. (Heeger, 2013). Most high-performance cells have thickness measurements of less than 100 nm, which is too thin to be processed reproducibly at high printing rates without

formation of pinholes (Li, 2013). However, in order to increase active layer thickness without drastically decreasing the PCE of the cell, it is necessary to optimize the morphological structure (He, 2012; He, 2015; Green, 2015; Etxeberria, 2015; Li, 2016; Zhang, 2017; Hoope, 2007). Upon formation of the electron-hole pair, it can travel only a distance of 10-15 nm before recombining and being lost as energy (Schmidt-Hansberg, 2011; Heeger, 2013; Zhang, 2017). Therefore, the amount that the charge carriers travel before reaching the electrodes must be limited as much as possible. The ideal active layer structure that successfully minimizes charge recombination rate utilizes columns, as depicted in **Figure 1.**

A form of morphology control that can be used to create this columnar active layer structure is the addition of an immiscible polymer that will induce a lateral phase separation during spin coating (Walheim, 1997; Wang, 2004; Heriot, 2005; Dunbar, 2010; Pan, 2012). As described by Walheim, the solvent evaporates as the polymers are spin coated, and the less soluble polymer will be depleted of solvent last, which, at sufficiently high polymer concentrations, will cause it to rise above the more soluble polymer and form columns (Walheim, 1997; Heriot, 2005). Furthermore, the polymer domain with the higher surface tension will take on a convex shape, whereas the polymer with lower surface tension will have a concave shape (Waldheim, 1997; Wang, 2004). This self-assembly process is illustrated in **Figure 2**. It is upon concave laterally segregated polymer domains that a more ideal polymer active layer structure can be templated. A previous study confirmed the use of this self-assembly process in the P3HT:PCBM active layer using polystyrene as a column-forming additive (Pan, 2011). There remains, however, much work to be done in developing ternary active layer blends with optimum morphology, as the efficiencies of self-templated polymers should still be

improved, and the self-assembly process during film formation is highly dependent on the species present in the solute-solvent system (Schmidt-Hansberg, 2011).

The purpose of this project is to develop the role of poly(methyl methacrylate) (PMMA) as a morphology-enhancing additive in the P3HT:PCBM active layer blend—specifically, by thickening the active layer and improving morphology. PMMA stood out as a good candidate after a collection of polymers were compared for solubility in chlorobenzene, surface tension, cost, and strength. Based on these characteristics, the active layer is expected to thicken due to the strength of PMMA and an increase in polymer blend concentration. Furthermore, based on surface tension, concave columns of PMMA within the active layer are expected to form, improving the PCE of the sample relative to a control. After verification of the columnar morphology and observation of the dramatic increase in EQE, reflection within the active layer was considered as an additional mechanism for raising absorbance and increasing the cell efficiency. The success of this approach to engineering an enhanced morphology of the active layer confirms a robust method for improving efficiency and scalability of polymer solar cell devices.

2. Materials and Methods:

All procedures listed below were performed by competition entrants after training, unless otherwise specified.

2.1. Materials.

Poly(methyl methacrylate) (MW = 27.5K), poly(3-hexylthiophene) (MW = 50-70K), 1-[3-(Methoxycarbonyl)propyl]-1-phenyl-[6.6]C_{61} (PCBM) (MW = 910.9), chlorobenzene, TiO_2, ethanol, acetone, silicon wafers, indium tin oxide glass, and microscope slide glass.

2.2 ***Survey of Potential Polymer Additives***

A survey of potential polymer additives was conducted with an eye to morphology control and practicality for commercialization based on solubility of the additive in chlorobenzene, surface energy, cost, and material properties.

A polymer that is soluble in chlorobenzene is sought in order to ensure ideal conduction in the organic semiconductor film. However, care must be taken in order to ensure that the additive is less soluble than P3HT:PCBM in chlorobenzene, and will form columns. The Hansen solubility parameters for the set of polymers were found, which divide the cohesive energy of a material into three components based on dispersion (δ_D), polarity (δ_P), and hydrogen bonding (δ_P), and can be used to predict solvation if a solute molecule and a solvent are within an adequate range by visualizing these parameters in three dimensions using the equation

$$(Ra)^2 = 4(\delta_{D1} - \delta_{D2})^2 + (\delta_{P1} - \delta_{P2})^2 + (\delta_{H1} - \delta_{H2})^2, \qquad [1]$$

in which Ra gives the location of the polymer in 3D space. When paired with the interaction radius R_o of the polymer, an empirically derived value, the likelihood for solvation of the polymer in the solvent can be approximated using the relative energy difference of the system:

$$RED = R_a/R_0 \qquad [2]$$

If RED < 1, then the molecules are alike and will dissolve; if RED = 1, the system will partially dissolve; and if RED > 1, the system will not dissolve. In this manner, the solvation of polymers in chlorobenzene was predicted.

Furthermore, the additive should have a surface energy higher than that of P3HT:PCBM to promote a concave shape in the separated polymer domains. Finally, the polymer should be cheap and sturdy in order to improve stability and thickness of the polymer films, and to make

the polymer solar cell more easily mass-produced. Through this process, PMMA was found as the best candidate for testing.

2.2. Preparation of P3HT:PCBM controls.

P3HT:PCBM solutions of 10:10 and 20:20 mg/mL were created. In this standard active layer blend, P3HT serves as the electron donor and PCBM the electron acceptor. 20 and 40 mg respectively of P3HT were added to 2 mL of chlorobenzene and placed on a magnetic stirrer for 18 hours. Then 20 and 40 mg respectively of PCBM were added and dissolved with stirring for 4 hours. The P3HT:PCBM thin films for morphology characterization were spin cast onto 1 cm^2 glass substrates at 1,000 rpm for 45 seconds with an acceleration of 1,000 rpm/s using a photoresist spinner (Headway Research Inc, 1-PM107D-R485).

2.3 Preparation of P3HT:PCBM solutions with PMMA additives.

The active layer solutions with PMMA as an additive were created with PMMA:P3HT: PCBM in a 10:10:10 mg/mL, 20:20:20 mg/mL, and 30:30:30 mg/mL. First, 20 mg, 40 mg, and 60 mg of PMMA were measured and placed into separate vials. These were then dissolved in chlorobenzene by heating on an oven at 80℃ for 6 hours. Then, the respective amounts of P3HT and PCBM were dissolved in the resulting solutions successively under stirring for 12 hours each.

2.4 Formation and Characterization of PMMA:P3HT:PCBM Morphologies.

PMMA:P3HT:PCBM solutions of 10:10:10 mg/mL, 20:20:20 mg/mL, and 30:30:30 mg/mL were spin cast at 1,000 RPM for 45 seconds with an acceleration of 1000 RPM/s. The film thicknesses were determined using a Rudolph three wavelength ellipsometer. The sample morphologies were characterized by using an Atomic Force Microscope (AFM) to take images in contact and conducting mode in order to find the topography, modulus, and conduction of the

sample. UV-Vis spectrophotometry using an Evolution 220 (Thermo Fisher Scientific, Shanghai, China) spectrometer on a 300-800 nm window relative to a glass control was performed to determine the absorption window and absorbance of the samples.

2.5 Device fabrication.

For devices fabricated, an inverted architecture polymer solar cell was created. The transparent cathode was formed by spin casting TiO_2 onto ITO glass. The active layer solutions were subsequently spin casted onto the substrate. Gold was applied as the top contact using physical vapor deposition, in which the molten metal was evaporated in a vacuum and condensed onto the active-layer substrate. Silver paste was then applied to form the anode.

2.6 Power conversion efficiency and external quantum efficiency testing of devices.

A solar simulator at air mass (AM) 1.5 and intensity 1 sun (1,000 W/square meter) was used to calculate the PCE of the solar cell. A voltage was applied in parallel to the device and the current response was measured from either -1.5 to 1.5 V or -2 to 2 V. The EQE for each device was determined based on the intensity of incident monochromatic light and the current output.

2.7 Simulation of light absorption improvement by effect of columnar nanostructures.

Light absorption can be maximized by thickening the active layer; however, due to the low electron mobility of the organic solar cell, free-carrier collection decreases with increasing thickness. Improving light absorption at a fixed active layer thickness can alleviate this dilemma.

Our study showed that adding a PMMA additive to the P3HT:PCBM binary blend induces columnar nanostructures and significantly improves solar cell efficiency. Thus, it was hypothesized that the increase in efficiency could be attributed to increased light reflectance within the cell.

The aim was to use mathematical models to show how PMMA-induced columnar nanostructures increase efficiency. The model was simplified by examining a 2D cross section of the active layer, using parameters from experimental data. Given a fixed absorption medium P3HT:PCBM, efficiency can be increased by increasing the total distance that light travels through the active layer before exiting, as more photons can be absorbed.

The absorption of light is proportional to its intensity at a given wavelength. Upon reaching the PMMA:P3HT:PCBM interface, the intensity of light is calculated using

$$I = I_0 e^{-\alpha L} \quad [3]$$

where I_0 is the original intensity of incident light, α is the light absorption coefficient given a specific material, and L is the distance traveled by light.

After reaching the interface, the intensity of light reflected back into the P3HT:PCBM blend can be found using

$$I = RI_0 e^{-\alpha L} \quad [4]$$

where R is the PMMA interfacial reflectance value, a function of the incident angle.

Thus, for each beam of incident light, the total absorbed light intensity within the active layer is

$$I_{absorbed} = I_0(1 - e^{-\alpha L1}) + RI_0(1 - e^{-\alpha L2}) + \ldots \quad [5]$$

where L1 is the distance traveled from the incident point to the first point of reflection, L2 is the distance traveled from the first point of reflection to the second point of reflection, and so on. The total absorption of all simulated light is

$$I_{total} = \Sigma_{i=1}^{n} I_{absorbed} i \quad [6]$$

where n is the total number of simulated incident beams of light.

AFM images (**Figure 3A**) show variety in PMMA column diameters and distance between columns. Thus, two representative geometries were chosen to exhibit improvement in absorption dependent on morphology. Parabolic column cross sections were assumed based on a previous study (Li, 2017); in one situation, the average distance between the widest points of the internal columns was fixed at 1188 nm, the distance between the thinnest points of the internal columns at 1500 nm, and the thickness of the active layer at 158 nm, as shown in **Figure 8A**. In the second situation, the average distance between the widest points was fixed at 560 nm, the distance between the thinnest points at 810 nm, and the thickness of the active layer at 158 nm, as shown in **Figure 8B**. Light was discretized to enter the cell at 1 nm intervals along its surface at angles ranging from 1 to 90 degrees. The system is symmetric; thus, this simulates all possibilities of light entering at any point and in any direction.

Assuming non-polarized light, the PMMA:air interfacial reflectance value R as a function of incident angle was found from the PMMA reflectance curve for incident angles less than the critical angle (Polyanskiy, N. M.). Past studies do not present values for a PMMA:P3HT:PCBM specific interface, but we assume a similar reflectance curve. The critical angle can be found by

$$\Theta = \frac{n_2}{n_1} \qquad [7]$$

where n_2 is the index of refraction of PMMA, 1.4893 (Polyanskiy, N. M.), and n_1 is the index of refraction of P3HT:PCBM, 1.83 (Lee W. H., 2010). At incident angles above the critical angle, total internal reflection of light occurs.

Solar radiation consists of a range of wavelengths and the absorption coefficient is dependent on wavelength. From the P3HT:PCBM UV-vis absorption coefficient spectra (Mihailetchi, 2006), one can make a reasonable simplification for an average α value of 3.5 x

10^{-6}/m for light wavelengths ranging 300-650 nm, above which absorption drops to almost 0. Improvement in PCE and EQE is proportional to the ratio of absorbance with columnar nanostructures to absorbance in a uniform binary blend.

Using these assumptions, a simulation model was built in C++ (source code can be found in references).

3. Results and Discussion:

3.1 Polymer Additive Survey

Using the calculated values for RED depicted in **Table 1**, the list of viable polymers was narrowed down to polystyrene, PMMA, PVA, and PEG based on solvability in chlorobenzene -- a polymer can be dissolved if RED < 1. Of these four, PMMA stands out for its excellent material properties -- it is strong, low weight, thermally stable, and cheap (Koleva, n.d.) Furthermore, its surface energy of 41 mN/m is high compared to the surface energy of P3HT:PCBM (19.7 mN/m), which suggests the formation of concave columns (Qin, 2014). PEG also stands out as a strong candidate for its high crystallinity, suggesting that it may act as a nucleation agent for more pure polymer domains (Zhang, 2017). However, the solubility parameters for PEG were found under heating for the polymer, suggesting that its solvability in chlorobenzene may actually be quite poor (Hansen, 2007). Preliminary tests of dissolving PEG in chlorobenzene showed that even at concentrations of .2 mg/mL, the PEG would not easily dissolve within the system. Therefore, the PMMA shows the greatest deal of potential as an additive.

3.2 Formation and morphology of the PMMA:P3HT:PCBM active layers.

First, the impact of PMMA on active layer thickness was observed for varying concentrations using ellipsometry measurements. As highlighted in **Table 2**, PMMA was found to increase film thickness: the thickness of the PMMA:P3HT:PCBM control at 10 mg/mL was 1,599 Å, an increase of 84.9% relative to the P3HT:PCBM control at the same concentration. Likewise at 20 mg/mL, the PMMA thin films measured 2,653.5 Å, in contrast to the 2038 Å control, a 30.2% increase. This result is an improvement on the active layer structure because thicker films demonstrate improved absorption and are more readily manufactured using mass-production techniques (Li, 2013).

The morphology of the PMMA:P3HT:PCBM active layer film was evaluated using contact and conduction mode AFM imaging. The height sensor setting, shown in **Figure 3A**, demonstrated a thin film containing regular columns within a homogenous blend. The columns reached about 300 nm in the 10:10:10 mg/mL sample and 500 nm in the 20:20:20 mg/mL sample, with diameters ranging from 3-10 μm and the widest columns having a slight concavity at the peak, shown in the height mapping in **Figure 3B**. This topography is indicative of a Volmer-Weber island morphology, in which the smallest stable molecule clusters are more strongly bound to each other than the substrate, thus growing in the z-direction to form islands (Ohring, 2001). These columns were hypothesized to be PMMA, which was verified using the DMT Modulus mapping setting of the AFM. The Young's modulus of PMMA is about 3.7 GPa (Young, 2011) whereas P3HT:PCBM mixtures have a Young's modulus of 1.6 or lower (Awartani, 2012). The columns have a much greater contact stiffness, approaching 3.7 GPa, therefore indicating the presence of PMMA (**Figure 4**). Areas of lower modulus within the

islands indicate the presence of P3HT, but this has no adverse effects on the performance of the ternary blend.

The segregation of PCBM at the boundary between PMMA and P3HT was confirmed by the presence of a ring of enhanced charge conduction at the interface (**Figure 5).** PCBM decreases the surface energy between PMMA and P3HT and thus reduces tension at the polymer interface (Li, 2011). This morphology is thus hypothesized to reduce the charge recombination rate by offering a direct path for charge conductors to the electrodes because the occupation of the interface by PCBM forms electron donor-acceptor channels, allowing for better charge transport.

3.3. Spectral absorbance of solar cells.

PMMA as an active layer blend additive was found to have no significant impact on the absorbance window of the active layer, as seen in **Figure 6.** Within the 300 to 800 nm range at which the absorbance was measured, all of the P3HT:PCBM and PMMA:P3HT:PCBM samples had significant absorption between 300 and 638 nm, with negligible improvement of the spectral absorbance range. However, at both the 10:10 mg/mL and 20:20 mg/mL concentrations, absorbance of the thin films with PMMA as a ternary polymer was found to be enhanced, likely as a result of the increased film thickness.

After normalization of the data set, the absorbance of each sample was integrated in order to compare the absorption across the four samples. At a concentration of 10:10 and 10:10:10 mg/mL, the addition of PMMA showed only moderate enhancement of light absorption, with a 4.7% increase between 300 and 800 nm. However, as the concentration, and hence the thin film

thickness, was increased to 20:20 and 20:20:20 mg/mL, the blend with PMMA had a 106.4% greater absorption relative to its counterpart.

3.4. PCE and EQE.

The first set of devices fabricated and tested were the PMMA:P3HT:PCBM cell and a P3HT:PCBM control. The PMMA and control cells were made with 20 mg/mL of each polymer. As highlighted in **Figure 7A,** the control achieved a PCE of 1.57% while the PMMA cell obtained a 2.1% PCE, a 33.75% improvement in efficiency.

With the determination that PMMA as an additive exhibited better cell performance, the second batch of samples focused on the PMMA:P3HT:PCBM solar cell and contained four samples, with two P3HT:PCBM controls, at 20 mg/mL ratios in order to determine whether the enhanced morphological and absorption characteristics would lead to a greater PCE. As shown by **Figure 7B**, the average PCE for the P3HT:PCBM devices was 2.105% while the average for the PMMA solar cell was 2.51%. This represents a 19.24% improvement in PCE while also showing greater overall PCE when compared with the batch one cells.

Furthermore, as shown in **Table 3**, the short circuit current density J_{sc} and the open-circuit voltage V_{oc} increased for the samples with PMMA as a third polymer. J_{sc} is the current density through the solar cell at zero voltage and in an ideal cell, it represents the maximum current that can be drawn from the device (He, 2011). The increase in short circuit current density for the PMMA:P3HT:PCBM samples, a 68.7% improvement in batch 1 and a 12.6% improvement in batch 2, shows enhanced function due to the addition of PMMA to the control P3HT:PCBM blend. The open-circuit voltage, V_{oc}, is the maximum voltage available from a solar cell and is a measure of the amount of recombination within a device (Chen, 2009).

Therefore, the 6.2% increase in V_{oc} of the PMMA:P3HT:PCBM cell in batch 1 and 7.4% increase in batch 2 highlights the effectiveness of PMMA as a ternary additive in improving recombination within a solar cell, and hence improving efficiency.

External quantum efficiency (EQE), which is the ratio of charge carriers to incident photons, was also shown to increase with the addition of PMMA, as shown in the last column of **Table 3,** where the PMMA:P3HT:PCBM sample exhibited an improvement of 68.0% relative to its control. Simulations were thus run in order to determine what aspect of the PMMA:P3HT:PCBM ternary blend would increase the EQE by such a large amount. One hypothesized theory was internal reflectance, where, due to the previously observed column formation of PMMA, it was thought possible that incident photons were being trapped within the columns and thus generating additional excitons.

3.5. Simulated increase in light absorption.

As described in **Section 2.7**, simulations were run in order to determine the effect of internal reflection between the PMMA columns on the PCE and EQE. In the first situation where columns were farther apart, a 5.5% increase in absorbed light intensity was observed. In the second situation with smaller spacing between columns, a 13.3% increase was observed. This clearly shows that enhancement in light absorption is directly dependent on ternary blend morphology. Increased light absorption contributes to improvement in PCE and EQE through $EQE = IQE * (1 - reflection - transmission)$, where IQE is the internal quantum efficiency, which affirms experimental results and demonstrates light trapping as a method of improved efficiency at a fixed active layer thickness. This model is a useful tool for guidance in future exploration of morphology optimization.

4. Illustrations:

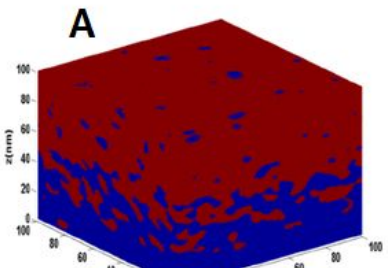

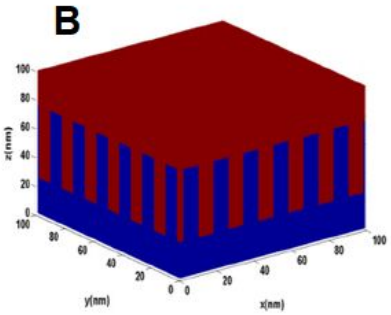

Figure 1. Comparison of disordered active layer solar cell with ideal ordered columnar structure. The columns allow for efficient charge carrier transport to the electrodes. Adapted from Maqsood, et. al., 2013. dx.doi.org/10.1021/jp406073y

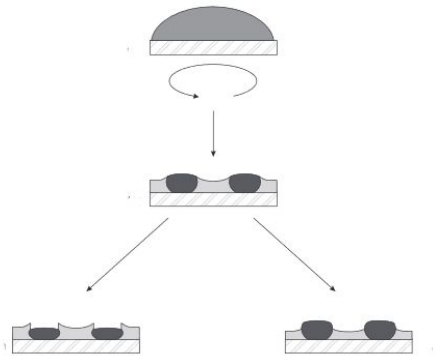

Figure 2. Depiction of formation mechanism for thin film of two immiscible polymers upon spin coating. The polymer domains separate based on different solubilities in the solvent, with the more soluble polymer going into the solid phase first and collapsing below the less soluble one. The polymer with the higher surface energy forms convex domains and that with lower surface energy forms concave domains, as shown by the light and dark polymer respectively. Adapted from Walheim, et al., 1997.

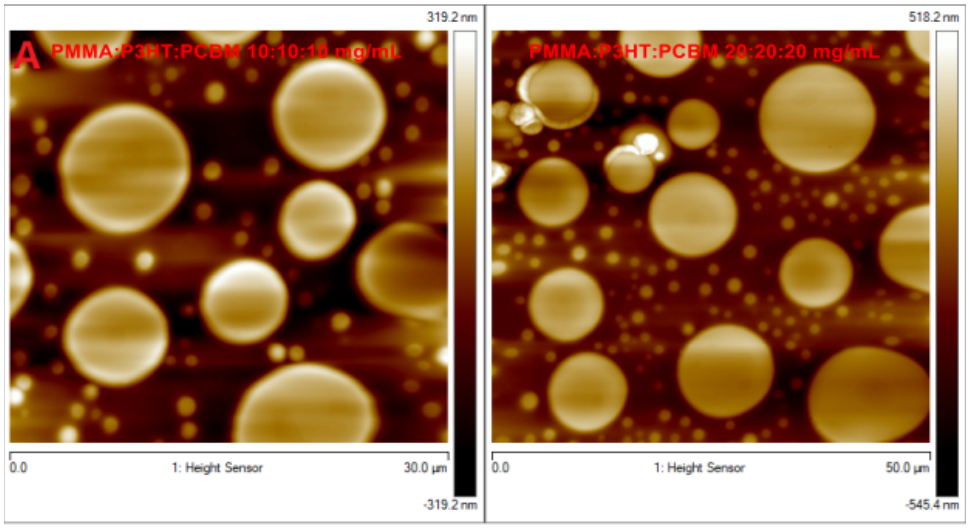

Figure 3. Atomic force microscopy (AFM) is used to capture images of 10:10:10 mg/mL and 20:20:20 mg/mL PMMA:P3HT:PCBM thin films under height sensor, contact mode. The figure shows a height profile of the thin film active layers within a 30.0 μm^2 and 50.0 μm^2 area. **(A)** The AFM images show that at both concentrations, the PMMA formed columns within the active layer that ranged in diameter from 3 - 10 µm. Furthermore, at 10 mg/mL **(Left)**, the columns reached peaks of 300 nm and at 20 mg/mL **(Right)**, they peaked at an average of 500 nm. The images show height with white being peaks and black troughs and a smooth gradient in between. **(B)** A cross section of the 10:10:10 mg/mL sample with height on the y-axis and horizontal length on the x-axis shows the existence of wide peaks with columnless regions between them. Furthermore, each peak is shown to have a depression of 70-100 nm at its peak.

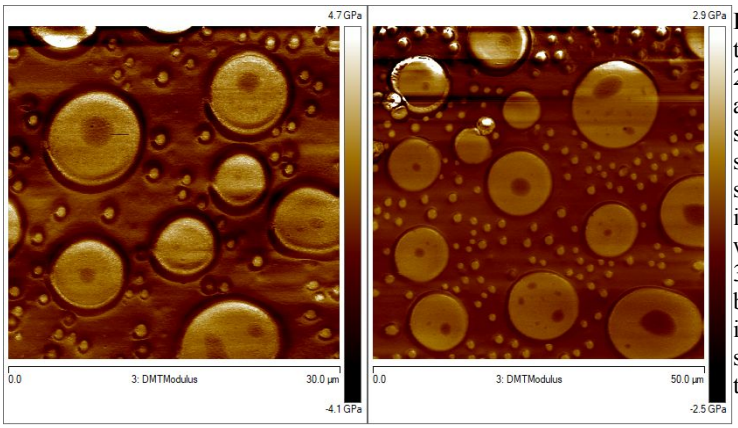

Figure 4. Contact mode AFM is used to determine the DMT modulus of the 10:10:10 **(Left)** and the 20:20:20 mg/mL **(Right)** PMMA:P3HT:PCBM active layer thin films. For both samples, the contact stiffness of the columns, between 3 and 4 GPa, is significantly greater than that of the blend, which stays near an average of 1.6 GPa. Therefore, this implies that the columns are formed by the PMMA, which is known to have an average modulus of about 3.7 GPa, phase segregated within a P3HT:PCBM blend. Furthermore, the centers of all large columns in both samples were found to contain regions of low stiffness, indicating the presence of P3HT within them, which has no effect on columnar refraction.

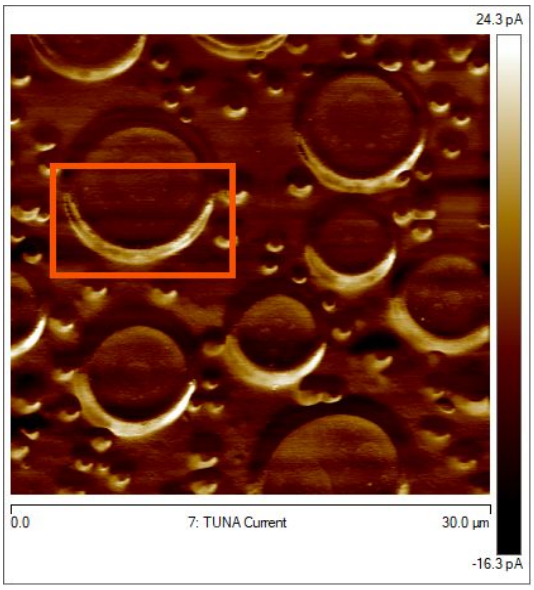

Figure 5. Conducting mode AFM is used to find areas of greater charge conduction by utilizing the TUNA current mode. In the 20:20:20 mg/mL PMMA:P3HT:PCBM sample shown, regions of greatest conductivity are in white while non conducting regions are shown in brown and black. The image shows that the columns themselves are predominantly non conducting, which supports the theory that PMMA, an insulating polymer, is what forms these columns. Furthermore, as highlighted in the orange popout, columns of PMMA are shown with conducting rings around their edges, which is hypothesized to be the segregation of PCBM into the interface between PMMA and P3HT, which could increase conductivity.

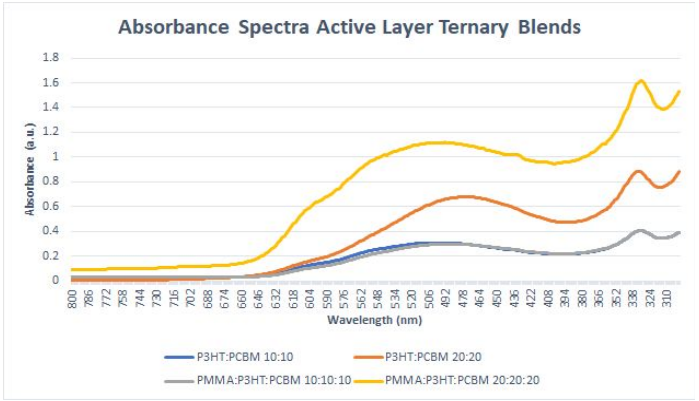

Figure 6. Ultraviolet-visible spectroscopy was used with wavelengths between 300 and 800 nm in order to characterize the absorption of the devices. Two concentrations, 10 mg/mL of each polymer and 20 mg/mL of each polymer, were tested with a P3HT:PCBM control and PMMA:P3HT:PCBM ternary blend. The 10:10:10 mg/mL ternary blend with PMMA **(blue)** showed marginal improvement over the control cell of the same concentration **(grey)** while the 20:20:20 mg/mL cell **(yellow)** exhibited significantly greater absorption relative to the control cell **(orange).** Integrating the curves to find total relative absorbance showed an improvement of 4.23% for the 10:10:10 PMMA:P3HT:PCBM cell and an improvement of 106% for the 20:20:20 PMMA:P3HT:PCBM cell. Finally, the inclusion of a third polymer (PMMA) was shown to not have any effect on the absorption window as all four samples absorb light the most between 646 and 300 nm.

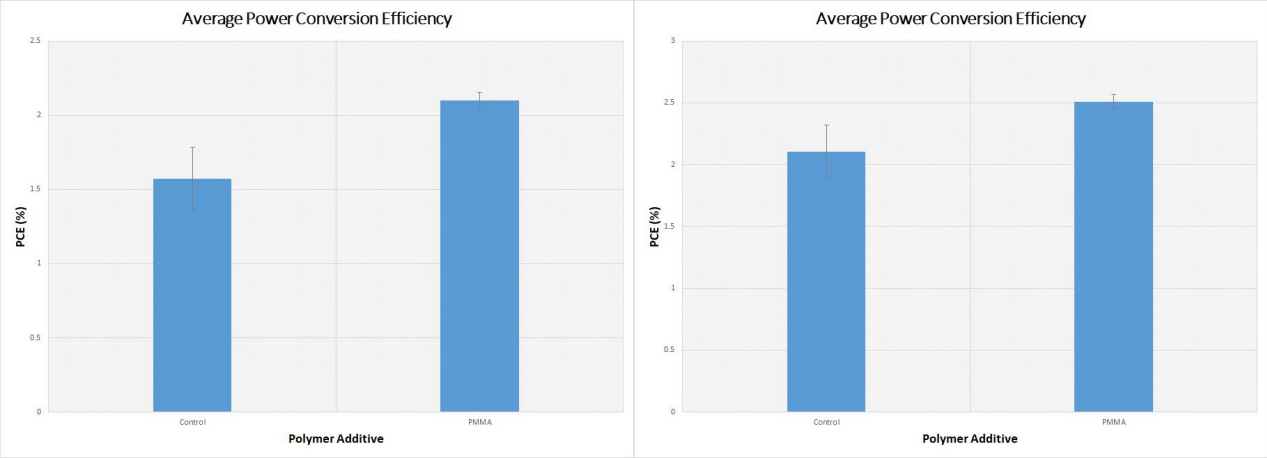

Figure 7. A (left) The PMMA:P3HT:PCBM active layer blends were tested under a solar simulator at AM 1.5 and intensity 1,000 W/m^2. The figure shows the power conversion efficiency (PCE) of the initial batch of photovoltaic devices, which is calculated by applying a voltage in parallel to the devices and measuring the current response within -1.5 to 1.5 V. The PCE of the ternary blend with PMMA (bar on right) was shown to be improved by 33.75% (from 1.57% to 2.1%) in comparison to the control. Furthermore, the standard error in the measurement of the PMMA:P3HT:PCBM cell was lower than that of the control P3HT:PCBM cell. **B (right)** The figure shows the PCE of the final batch of photovoltaic devices, which is calculated by applying a voltage in parallel to the devices and measuring the current response within -2.0 to 2.0 V. The PCE of the ternary blend with PMMA (bar on right) was shown to be improved by 19.24% (from 2.105% to 2.51%) in comparison to the control.

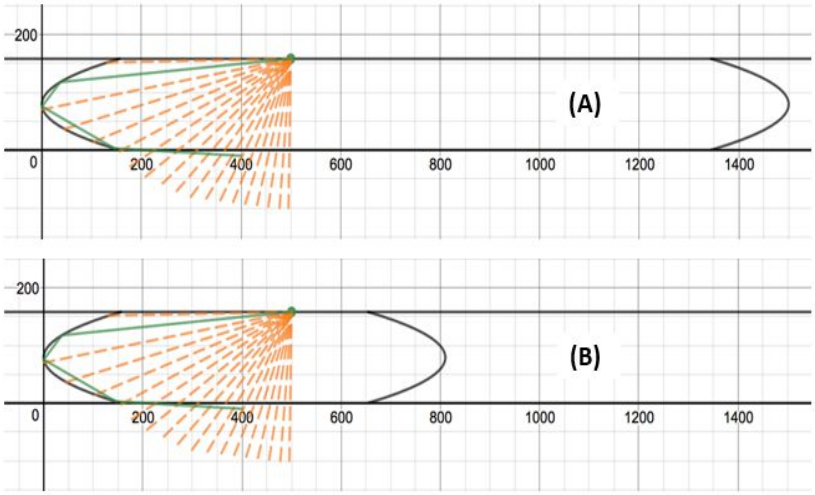

Figure 8: This figure shows the two situations simulated in the model – **(A)** with more space between PMMA columns and **(B)** with closer PMMA columns. The distance between the PMMA columns is altered in order to determine the effect on light reflection. Incident light from one point along the surface is depicted here, with dashed lines as incident rays. The solid green line traces the path of one example ray as it reflects within the active layer due to columnar nanostructures.

Polymer	RED with Chlorobenzene	Surface Energy (mN/m)*	Cost per gram†
PS	0.43	40.7	$1.90
PMMA	0.6	41	$0.25
PVA	0.8	37	$1.52
PEG	.94*	41.5	$2.74
PES	1	48	$1.40
PVC	1.2	39	$0.22
PA	1.5	46.5	$1.65
PTFE	1.6	19	$1.40
PVDF	2.9	25	$0.97

Table 1. Data for solubility, surface energy, and cost per gram for nine polymers are tabulated. The RED, or relative energy difference, is calculated using Hansen solubility parameters as described in the methods, and predicts solubility of a polymer in chlorobenzene through the relation RED < 1 being a soluble polymer. In this manner, PS, PMMA, PVA, and PEG are isolated as candidates for polymer additive. The surface energies describe the shape that the separated polymer domain will take, with surface energies larger than 19.7 mN/m being conducive to concave. Finally, cost per gram is listed, with cheaper polymers being more preferable.
Hansen solubility parameters were obtained from Hansen, Charles M. *Hansen solubility parameters: a user's handbook*. CRC press, 2007.
† Stock pricing obtained from Sigma Aldrich.

Active Layer Blend	Concentration (mg/mL)	Thickness (Å)
Control	10	864.5
	20	2038
PMMA	10	1599
	20	2653.5
	30	3448.5

Table 2. A Rudolph three wavelength ellipsometer was used to calculate the thickness of control (P3HT:PCBM) films and PMMA:P3HT:PCBM thin films at concentrations of 10 mg/mL, 20 mg/mL, and 30 mg/mL (only for the PMMA sample) of each polymer. The thicknesses obtained showed an 84.9% increase in the thickness of the 10:10:10 mg/mL films and a 30.2% increase in thickness of the 20:20:20 mg/mL films with PMMA. The increased thickness of the films with the addition of PMMA is significant because it allows for potential mass-production through roll-to-roll manufacturing, for which the thinness of organic solar cell active layers is a limitation.

	Sample	J_{sc} (mA/cm^2)	V_{oc} (V)	FF (%)	PCE (%)	EQE (%)
Batch 1	control	6.27	0.565	40.5	1.57	
	with PMMA	10.58	0.600	33.1	2.10	
Batch 2	control	8.73	0.540	47.9	2.11	20.6
	with PMMA	9.83	0.580	46.2	2.51	34.6

Table 3. Device parameters for the two batches of solar cells tested are shown. J_{sc} is short circuit current, V_{oc} is open current voltage, FF is fill factor, PCE is power conversion efficiency, EQE is external quantum efficiency. In both batches, the PCE of the PMMA:P3HT:PCBM active layers was greater than those of the control P3HT:PCBM active layers. Furthermore, the EQE, which was only calculated in batch 2, showed a 68% increase with the addition of PMMA, indicating light trapping as a possible explanation. Furthermore, J_{s},, which is the current density through the solar cell when the voltage across it is zero and represents the maximum theoretical current that can be drawn from the device, increased with the addition of PMMA. Likewise, V_{oc} which is the maximum voltage available from a solar cell and is a measure of the amount of recombination within a device, increased by 6.2% and 7.4% in batch 1 and 2 respectively.

5. Conclusions and Future Work:

The PMMA:P3HT:PCBM active layer blend used to form polymer solar cells demonstrated an increased film thickness, improved power conversion efficiency over the P3HT:PCBM controls, and enhanced light absorption within the 300 to 800 nm range through internal reflections, all of which points to dramatic improvements in scalability and efficiency in the devices. The PMMA-enhanced films showed greater thickness at both 10 mg/mL and 20 mg/mL concentrations, showing that organic polymer solar cells with a ternary PMMA blend are far more applicable for mass production through inexpensive roll-roll manufacturing. Although thickness was increased, efficiency was still preserved by limiting charge-recombination rate through clear column morphology, as demonstrated in atomic force microscopy images. Finally, the EQE of ternary solar cells was shown to be greater than that of P3HT:PCBM cells and simulation of light reflection between the columns confirmed the hypothesis that reflection plays

a key role in the EQE increase. Thus, this project is a key step towards creating polymer solar cells that are efficient and mass-producible, which can lead in the future to low-cost, ultra-portable solar energy.

In the future, a wider survey of potential polymer additives using the methods described will be helpful for determining other likely candidates for testing. In addition, cross-section and top-view transmission electron microscopy (TEM) should be conducted in order to determine the exact structure of the PMMA columns and refine the light reflectance model. The PCE and EQE data were taken with only two batches, with the EQE calculated only for the final batch. More samples should be run in order to reduce statistical variance, eliminate the effect of possible outliers due to laboratory conditions and environmental factors. In order to demonstrate morphology optimization as a general effective method of improving solar cell performance, PMMA should be tested with a variety of polymer-fullerene active layer blends in order to determine whether the benefits of column formation and lower exciton recombination can be extended beyond P3HT:PCBM Finally, a C++ model was developed to simulate light trapping within the photoactive layer, demonstrating enhanced light absorption in the presence of columnar nanostructures, and showing that increase in quantum efficiency is dependent on morphology. In the future, a 3D version of the model will be developed to more accurately predict improvement. In addition, parameters will be generalized to test a variety of column shapes and densities in order to optimize EQE, as a direction for experimental design.

References:

Source code:
https://github.com/competitionentrant0/PMMA-Additive-Induced-Active-Layer-Self-Assembly-in-Polymer-Solar-Cell
Username: competitionentrant0
Password: CoolSolarCell0

Awartani, O., Lemanski, B. I., Ro, H. W., Richter, L. J., DeLongchamp, D. M., & O'Connor, B. T. (2013). Correlating stiffness, ductility, and morphology of polymer: fullerene films for solar cell applications. *Advanced Energy Materials*, *3*(3), 399-406.

Blom, P. W., Mihailetchi, V. D., Koster, L. J. A., & Markov, D. E. (2007). Device physics of polymer: fullerene bulk heterojunction solar cells. *Advanced Materials*, *19*(12), 1551-1566.

Brabec, C. J., Heeney, M., McCulloch, I., & Nelson, J. (2011). Influence of blend microstructure on bulk heterojunction organic photovoltaic performance. *Chemical Society Reviews*, *40*(3), 1185-1199.

Chen, H. Y., Hou, J., Zhang, S., Liang, Y., Yang, G., Yang, Y., ... & Li, G. (2009). Polymer solar cells with enhanced open-circuit voltage and efficiency. *Nature photonics*, 3(11), 649-653.

Dang, M. T., Hirsch, L., Wantz, G., & Wuest, J. D. (2013). Controlling the morphology and performance of bulk heterojunctions in solar cells. Lessons learned from the benchmark poly (3-hexylthiophene):[6, 6]-phenyl-C61-butyric acid methyl ester system. *Chemical reviews*, *113*(5), 3734-3765.

Dennler, G., Scharber M., Brabec, C. "Polymer-Fullerene Bulk-Heterojunction Solar Cells." *Advanced Materials*. 21, 1323-1338.

[1] Edenhofer. The IPCC Special Report on Renewable Energy Sources and Climate Change Mitigation 24th September 2011, The New School for Social Research, New York Prof. Dr. Ottmar Edenhofer Co-Chair of the IPCC Working Group III "Mitigation of Climate Change

Etxebarria, I., Ajuria, J., & Pacios, R. (2015). Solution-processable polymeric solar cells: a review on materials, strategies and cell architectures to overcome 10%. *Organic Electronics*, *19*, 34-60.

Florian Machui, Stefan Langner, Xiangdong Zhu, Steven Abbott, Christoph J. Brabec, "Determination of the P3HT:PCBM solubility parameters via a binary solvent gradient method: Impact of solubility on the photovoltaic performance." *Solar Energy Materials and Solar Cells*, Volume 100, 2012, Pages 138-146, ISSN 0927-0248, https://doi.org/10.1016/j.solmat.2012.01.005

Green, M. A., Emery, K., Hishikawa, Y., Warta, W., & Dunlop, E. D. (2015). Solar cell efficiency tables (Version 45). *Progress in photovoltaics: research and applications*, *23*(1), 1-9.

Hansen, Charles M. *Hansen solubility parameters: a user's handbook*. CRC press, 2007.

Hansen, Charles. "Solubility in the coatings industry." *Skandinavisk Tidskriftfoer Faergoch Lack* 17.4 (1971): 69-77.

He, Z., Zhong, C., Huang, X., Wong, W.-Y., Wu, H., Chen, L., Su, S. and Cao, Y. (2011), Simultaneous Enhancement of Open-Circuit Voltage, Short-Circuit Current Density, and Fill Factor in Polymer Solar Cells. *Adv. Mater.*, 23: 4636–4643. doi:10.1002/adma.201103006

He, Z., Zhong, C., Su, S., Xu, M., Wu, H., & Cao, Y. (2012). Enhanced power-conversion efficiency in polymer solar cells using an inverted device structure. *Nature Photonics*, *6*(9), 591-595.

He, Z., Xiao, B., Liu, F., Wu, H., Yang, Y., Xiao, S., ... & Cao, Y. (2015). Single-junction polymer solar cells with high efficiency and photovoltage. *Nature Photonics*, *9*(3), 174-179.

Heeger, A. J. (2014). 25th anniversary article: bulk heterojunction solar cells: understanding the mechanism of operation. *Advanced Materials*, *26*(1), 10-28.

Hoppe, H., & Sariciftci, N. S. (2007). Polymer solar cells. In *Photoresponsive Polymers II* (pp. 1-86). Springer Berlin Heidelberg.

Hosoya M, Oooka H, Nakao H, Mori S, Gotanda T, Shida N, Saito M, Nakano Y, Todori K. Module development for polymer solar cells. Abstract O-PV-6-2, Grand Renewable Energy Conference, Tokyo, July 2014; 21–37.

Huang, Y., Wen, W., Mukherjee, S., Ade, H., Kramer, E. J., & Bazan, G. C. (2014). High‐Molecular‐Weight Insulating Polymers Can Improve the Performance of Molecular Solar Cells. *Advanced Materials*, *26*(24), 4168-4172.

Jo, J., Na, S. I., Kim, S. S., Lee, T. W., Chung, Y., Kang, S. J., ... & Kim, D. Y. (2009). Three‐Dimensional Bulk Heterojunction Morphology for Achieving High Internal Quantum Efficiency in Polymer Solar Cells. *Advanced Functional Materials*, *19*(15), 2398-2406.

Koleva, M. “Injection Moulding Materials, PMMA.” Cast Products and Mould Designer Skills at the European Context (n.d.). http://webhotel2.tut.fi/projects/caeds/tekstit/frame_materials.html

Lee, S., Nam, S., Kim, H., & Kim, Y. (2010). Organic solar cells with submicron-thick polymer: fullerene bulk heterojunction films. *Applied Physics Letters*, *97*(10), 103503.

Lee, W. H., Chuang, S. Y., Chen, H. L., Su, W. F., & Lin, C. H. (2010). Exploiting optical properties of P3HT: PCBM films for organic solar cells with semitransparent anode. Thin Solid Films, 518(24), 7450-7454. Chicago

Li, G., Zhu, R., & Yang, Y. (2012). Polymer solar cells. *Nature photonics*, *6*(3), 153-161.

Li, W., Hendriks, K. H., Roelofs, W. S., Kim, Y., Wienk, M. M., & Janssen, R. A. (2013). Efficient small bandgap polymer solar cells with high fill factors for 300 nm thick films. *Advanced materials*, *25*(23), 3182-3186.

Li, S., Ye, L., Zhao, W., Zhang, S., Mukherjee, S., Ade, H., & Hou, J. (2016). Energy‐Level Modulation of Small‐Molecule Electron Acceptors to Achieve over 12% Efficiency in Polymer Solar Cells. *Advanced Materials*, *28*(42), 9423-9429.

Li, Hongfei, et al. "A new strategy to engineer polymer bulk heterojunction solar cells with thick active layers via self-assembly of the tertiary columnar phase." *Nanoscale* 9.32 (2017): 11511-11522.

Li, Hongfei. "The Influence of the Columnar Structure in the Active Layer (PMMA/P3HT/PCBM) on the Performance of the Bulk Heterojunction Solar Cell." Unpublished Master's Thesis (2011). Stony Brook University, Stony Brook, New York.

Ma, W., Tumbleston, J. R., Wang, M., Gann, E., Huang, F., & Ade, H. (2013). Domain purity, miscibility, and molecular orientation at donor/acceptor interfaces in high performance organic solar cells: paths to further improvement. *Advanced Energy Materials*, *3*(7), 864-872.

Maqsood, I., Cundy, L. D., Biesecker, M., Kimn, J., Johnson, D., Williams, R., & Bommisetty, V. (2013). Monte Carlo Simulation of Förster Resonance Energy Transfer in 3D Nanoscale Organic Bulk Heterojunction Morphologies. *Journal of Physical Chemistry,* 117(41), 21086-21095.

Mihailetchi, Valentin & X. X. Xie, H & de Boer, B & Koster, L & Blom, Paul. (2006). Charge Transport and Photocurrent Generation in Poly(3‐hexylthiophene): Methanofullerene Bulk‐Heterojunction Solar Cells. Advanced Functional Materials. 16. 699 - 708. 10.1002/adfm.200500420.

Miller-Chou, Beth A., and Jack L. Koenig. "A review of polymer dissolution." *Progress in Polymer Science* 28.8 (2003): 1223-1270.

Pan, C., Li, H., Akgun, B., Satija, S. K., Zhu, Y., Xu, D., Ortiz, J., Gersappe, D., Rafailovich, M. H. (2013). Enhancing the efficiency of bulk heterojunction solar cells via templated self-assembly. *Macromolecules*, *46*(5), 1812-1819.

Peet, J., Wen, L., Byrne, P., Rodman, S., Forberich, K., Shao, Y., ... & Waller, D. (2011). Bulk heterojunction solar cells with thick active layers and high fill factors enabled by a bithiophene-co-thiazolothiazole push-pull copolymer. *Applied Physics Letters*, *98*(4), 15.

Qin, Dashan & Wang, Wenbo & Wang, Mingxia & Jin, Song & Zhang, Jidong. (2014). The dependence of the cathode architecture on the photoactive layer morphology in bulk-heterojunction polymeric solar cells. Semiconductor Science and Technology. 29. 125011. 10.1088/0268-1242/29/12/125011.

Scharber, M. C., & Sariciftci, N. S. (2013). Efficiency of bulk-heterojunction organic solar cells. *Progress in polymer science*, *38*(12), 1929-1940.

Schilinsky, P., Waldauf, C., & Brabec, C. J. (2002). Recombination and loss analysis in polythiophene based bulk heterojunction photodetectors. *Applied Physics Letters*, *81*(20), 3885-3887.

Schmidt-Hansberg, B., Sanyal, M., Klein, M. F., Pfaff, M., Schnabel, N., Jaiser, S., ... & Gerthsen, D. (2011). Moving through the phase diagram: morphology formation in solution cast polymer–fullerene blend films for organic solar cells. *Acs Nano*, *5*(11), 8579-8590.

Søndergaard, R., Hösel, M., Angmo, D., Larsen-Olsen, T., Krebs, F. "Roll-to-roll fabrication of polymer solar cells." *Materials Today*. 15(2), 36-49.

Watts, B., Belcher, W. J., Thomsen, L., Ade, H., & Dastoor, P. C. (2009). A quantitative study of PCBM diffusion during annealing of P3HT: PCBM blend films. *Macromolecules*, *42*(21), 8392-8397.

Heriot, S. Y., & Jones, R. A. (2005). An interfacial instability in a transient wetting layer leads to lateral phase separation in thin spin-cast polymer-blend films. *Nature materials*, *4*(10), 782-786.
Walheim, S., Böltau, M., Mlynek, J., Krausch, G., & Steiner, U. (1997). Structure formation via polymer demixing in spin-cast films. *Macromolecules*, *30*(17), 4995-5003.

Wang, P., & Koberstein, J. T. (2004). Morphology of immiscible polymer blend thin films prepared by spin-coating. *Macromolecules*, *37*(15), 5671-5681.

Yuan, Y., & Lee, T. R. (2013). Contact angle and wetting properties. In *Surface science techniques* (pp. 3-34). Springer Berlin Heidelberg.

Zhang, L., & Ma, W. (2017). Morphology optimization in ternary organic solar cells. *Chinese Journal of Polymer Science*, *35*(2), 184-197.